

---

# Synthesis, Properties, and Intermolecular Interactions in the Solid States of $\pi$ -Congested X-Shaped 1,2,4,5-Tetra(9-anthryl)benzenes

Tomohiko Nishiuchi,<sup>\*[a,b]</sup> Shino Takeuchi,<sup>[a]</sup> Yuta Makihara,<sup>[a]</sup> Ryo Kimura,<sup>[c]</sup> Shohei Saito,<sup>[c]</sup> Hiroyasu Sato,<sup>[d]</sup> and Takashi Kubo<sup>\*[a,b]</sup>

---

[a] Dr. T. Nishiuchi, S. Takeuchi, Y. Makihara, Prof. Dr. T. Kubo  
Department of Chemistry, Graduate School of Science, Osaka University  
1-1 Machikaneyama, Toyonaka, Osaka 560-0043 (Japan)  
E-mail: [nishiuchit13@chem.sci.osaka-u.ac.jp](mailto:nishiuchit13@chem.sci.osaka-u.ac.jp)

[b] Dr. T. Nishiuchi, Prof. Dr. T. Kubo  
Innovative Catalysis Science Division, Institute for Open and Transdisciplinary Research Initiatives, (ICS-OTRI), Osaka University  
Suita, Osaka 565-0871 (Japan)

[c] R. Kimura, Prof. Dr. S. Saito  
Department of Chemistry, Graduate School of Science, Kyoto University  
Kitashirakawa Oiwake, Sakyo, Kyoto 606-8502 (Japan)

[d] Dr. H. Sato  
Rigaku Corporation, 3-9-12 Matsubara, Akishima, Tokyo 196-8666 (Japan)

Supporting information for this article is given via a link at the end of the document.

**Abstract:** A Negishi coupling based synthesis of 1,2,4,5-tetra(9-anthryl)benzene derivatives, possessing X-shaped molecular structures, is described. The results of X-ray crystallographic analysis show that two-dimensional highly ordered packing structure of the crystalline state of the unsubstituted derivative is a consequence of intermolecular  $\pi$ - $\pi$  and CH- $\pi$  interactions between anthracene units. Photoirradiation of the unsubstituted derivative as a precipitated solution promotes intramolecular [4+4] photocycloaddition reactions between both adjacent pairs of anthracene units to produce a crystalline polycyclic product having a unique 1.700 Å long carbon-carbon single bond. Furthermore, charge-transfer complexes, displaying near-infrared absorption and emission, are generated by co-crystallization of the X-shaped unsubstituted member of the group with electron-acceptor molecules.

## Introduction

$\pi$ -Congested aromatic systems,<sup>[1,2]</sup> which have distances between two  $\pi$ -planes that are smaller than the sum of van der Waals (vdWs) radii of carbon (3.40 Å), have unique optoelectronic properties derived from through-space (TS)  $\pi$ -conjugation. For example, different from substances that contain non-interacting  $\pi$ -moieties,  $\pi$ -congested aromatic systems readily form excimers

formation even at room temperature and they undergo intramolecular photocycloaddition reactions between the interacting  $\pi$ -planes.<sup>[3,4]</sup> The interesting properties of  $\pi$ -congested systems make them fascinating targets not only for fundamental studies aimed at elucidating the origin and optoelectronic effects of TS  $\pi$ -conjugation but also for the development of novel organic electronic devices.

Recently, we introduced a new type of  $\pi$ -congested system, termed  $\pi$ -clusters,<sup>[5]</sup> which are composed of two and three interacting anthracene (Ant) units<sup>[6]</sup> (see **1a-b** and **2a-b** in Figure 1). The strategy employed to design these systems utilizes a rigid benzene scaffold to covalently position the Ant units within short distances. The effects of TS  $\pi$ -conjugation in the  $\pi$ -clusters comprised of two neighboring anthracene units bonded at *ortho*-positions of a benzene ring has been elucidated. In addition, we demonstrated that the unique 2D packing structure in the crystalline state of **2a** is a consequence of intermolecular  $\pi$ - $\pi$  and CH- $\pi$  interactions between the three radially arranged Ant units. This type of solid state molecular assembly is a distinctive feature of aromatic congested molecules such as the six-fold phenyl embracing, which is six-fold edge-to-face interactions of phenyl rings observed in tetraphenyl phosphonium and triphenylmethyl

cation dimers.<sup>[7,8]</sup> Furthermore, photoirradiation promotes intramolecular [4+4] cycloaddition reactions between neighboring Ant in units the respective di-Ant and tri-Ant substituted benzenes **1a** and **2a**, which can be thermally reversed. These photo/thermal properties enable these substances to undergo, light heat and mechanical stress stimulated color change responses.

In our continuing studies of  $\pi$ -congested molecules, whose ultimate aim is to explore the properties of hexa(9-anthryl)benzene (**HAntB**), we recognized that 1,2,3,4-tetra(9-anthryl)benzene (**3**) and 1,2,4,5-(9-anthryl)benzene (**4a**) would serve as key models to provide preliminary information about the physical properties of increasingly Ant-congested systems. However, tetra(9-anthryl) substituted benzenes, including the simple X-shaped 1,2,4,5-(9-anthryl) derivative **4a**, have not yet been described in the literature.<sup>[9]</sup> We believed that **4a** would be a good reference compound for the more crowded analog **3**, because it would enable us to develop ideal synthetic protocols, and to explore its crystal packing structure and crystalline state intramolecular photocycloaddition reactions.

In the study described below, we developed optimized conditions for a Pd(I)-catalyzed Negishi coupling process to generate the *n*-butyl (**4b**) and trimethylsilyl (**4c**) analogs, and a simple method for conversion of **4c** to the parent compound **4a**. An exploration to uncover the distinctive properties of these substances showed that the Ant units in **4a** have an X-shaped arrangement and that they engage in intermolecular  $\pi$ - $\pi$  and CH- $\pi$  interactions in the crystalline state that results in an interesting 2D packing structure. In addition, we observed that photoirradiation of **4a** generates the intramolecular photocycloaddition product **4a-PI**, which in its crystalline state contains an unusually 1.700 Å long C-C single bond. Finally, we observed that *n*-butyl substituted isomer **4b** undergoes charge-transfer (CT) complexation with acceptor molecules to produce unique CT crystals that display exciplex emission.

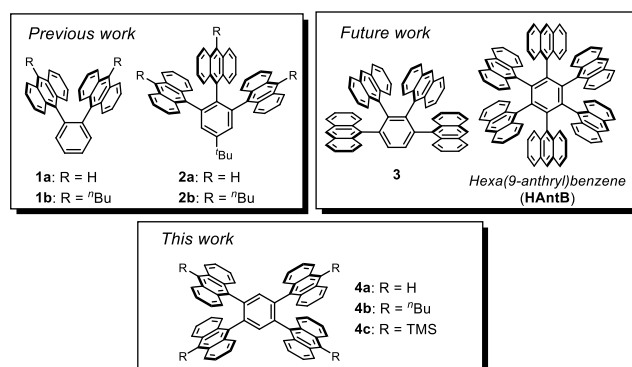
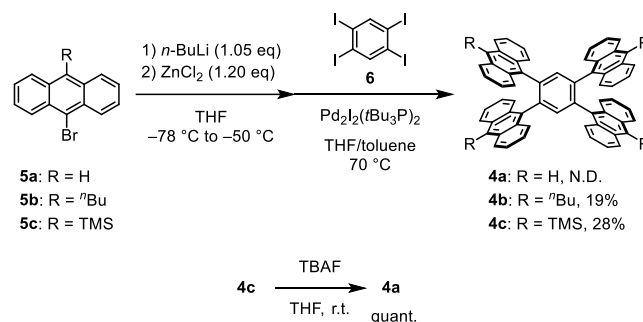


**Figure 1.** Anthracene based radial  $\pi$ -clusters. Respective 1,2-di- and 1,2,3-tri(9-anthryl)benzenes (**1a-b** and **2a-b**) (previous work, top left), 1,2,3,4-tetra(9-anthryl)benzene (**3**) and hexa(9-anthryl)benzene (**HAntB**) (future work, top right), and 1,2,4,5-tetra(9-anthryl)benzenes (**4a-c**) (this work, down).

## Results and Discussion

### Synthesis and structure elucidation

The synthetic routes used to prepare **4a-c** are shown in Scheme 1. Initially, we attempted to prepare **4a** by using Pd(I)-catalyzed Negishi coupling reaction between 9-bromoanthracene (**5a**) and tetraiodobenzene **6**.<sup>[10]</sup> However, we were unable to detect formation of **4a**, a likely consequence of its extreme insolubility. In contrast, using a similar coupling protocol with *n*-butyl (*n*Bu) and trimethylsilyl (TMS) substituted bromoanthracenes **5b-c** led to successful formation of the corresponding 1,2,4,5-(9-anthryl)benzenes **4b** and **4c** in respective 19% and 28% yields. The low efficiencies of these reactions, in comparison to the 90% yield of a similar process employed for the synthesis of the di-Ant derivative **1a**, is likely associated with the electron-donating and/or steric nature of substituents on the Ant units that negatively impacts oxidative addition of palladium species to the iodoarene. Importantly, we were able to generate **4a** quantitatively as pale yellow solid by TBAF promoted removal of the TMS group in **4c**.



**Scheme 1.** Synthesis of **4a-b**.

Single crystals of **4b** and **4c** suitable for X-ray crystallographic analysis were obtained by recrystallization from  $\text{CH}_2\text{Cl}_2/\text{EtOH}$  and  $\text{CHCl}_3/\text{EtOH}$ , respectively. Owing to insolubility issues (1-2 mg/100 mL in  $\text{CHCl}_3$  at room temperature), single crystals of **4a** could not be produced using direct recrystallization. However, crystals of **4a** can be generated by allowing a solution of **4c** in  $\text{CHCl}_3$  to stand for several days, conditions under which trace amounts of acidic species in the solvent serve as TMS deprotection agents. The crystalline state structures of **4a-c** are shown in Figure 2. The molecular structure of **4a** is  $C_i$  symmetric with the center of the benzene ring as the inversion point. The Ant-Ant intramolecular distances, corresponding to those between C9 and C9' ( $\text{C9}\cdots\text{C9}'$ ) and C10 and C10' ( $\text{C10}\cdots\text{C10}'$ ), are 3.06 and 6.25 Å, respectively. The dihedral angles between the Ant unit and the central benzene ring are 77.9° and 79.1°. On

the other hand, the molecular structure of **4b** has  $C_2$  symmetry with the axis of rotation in the longitudinal direction of the molecule, resulting in asymmetric intramolecular Ant-Ant distances  $C9_a \cdots C9_a'$  (3.01 Å),  $C9_b \cdots C9_b'$  (2.93 Å),  $C10_a \cdots C10_a'$  (5.61 Å) and  $C10_b \cdots C10_b'$  (5.17 Å). The dihedral angles between the *para*-disposed Ant units and the central benzene ring are 67.1° and 72.7°. In contrast to those of **4a**, the intramolecular C10-C10' distance in **4b** is 0.64-1.08 Å longer, and the dihedral angles of the Ant units are closer to 90°. These differences are likely associated with the lack of substituents on the four Ant units in **4a** which enables greater intermolecular CH- $\pi$  and  $\pi$ - $\pi$  contacts. Furthermore, the strong intermolecular interactions in **4a** lead to formation of a regularly arranged 2D packing structure (Figure 2c, Figure S1).

Like in **4b**, the absence of multiple intermolecular interactions in the TMS-analog **4c** leads to very short Ant-Ant intramolecular distances ( $C9 \cdots C9'$  and  $C10 \cdots C10'$  are 2.92 and 5.06 Å, respectively) (Figure 2d). Dihedral angles between the Ant unit and the central benzene ring in **4c** are 73.7° and 73.5°. The distinctive feature of the crystal structure of **4c** is a highly distorted Ant unit caused by the steric bulk of the TMS substituent.<sup>[11]</sup> The largest bent angle  $\theta$  of the Ant plane is 12.1° ( $\theta = 180^\circ - \angle C1-C9-C10$ ), which results in positioning C10 on the Ant unit 0.56 Å out-of-plane (Figure 2e). In addition, the distortion enables the TMS groups on adjacent Ant units to interact through dispersion forces, which results in further shortening of the Ant-Ant distance.

The results of computations using the B3LYP-D3 functional that includes a dispersion force term, nicely reproduce the crystal state structure of **4c**, whereas those using the B3LYP functional that lacks a dispersion force term give rise to a structure having a larger than observed Ant-Ant distance (Figure S6). Calculations on **4b'**, possessing R= Et group instead of <sup>t</sup>Bu group, using the B3LYP-D3 functional also lead to a structure that is close to that of **4b** observed in the crystalline state, indicating that large dispersion force between adjacent Ant-Ant units (Figure S7).

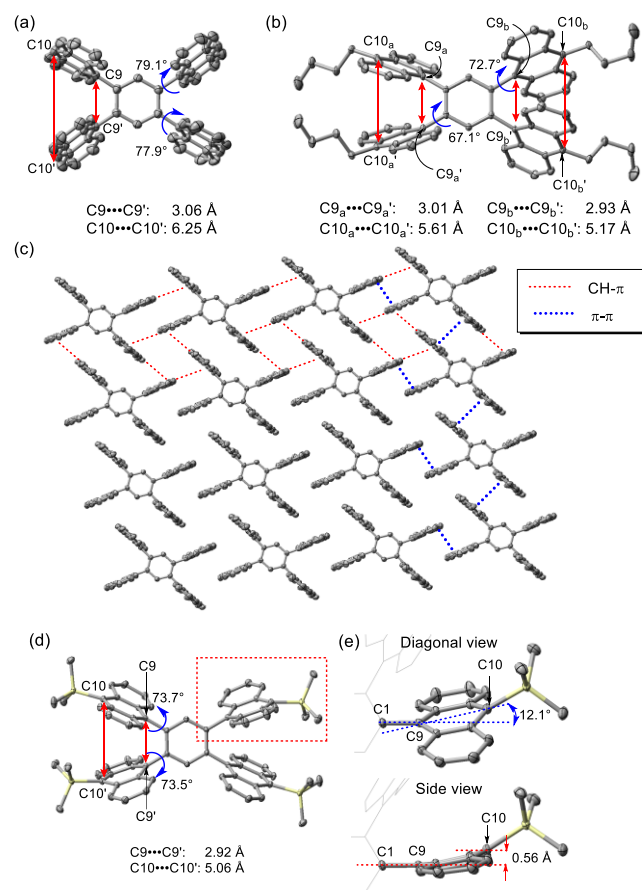


**Figure 2.** Crystalline state structures with intramolecular distances between face-to-face Ant units and a dihedral angle of Ant unit. (a) **4a**. (b) **4b**. (c) Packing structure of **4a**. Red-dashed line and blue-dashed line indicate CH- $\pi$  and  $\pi$ - $\pi$  interactions, respectively. (d) Intramolecular distances between faces of the Ant units and a dihedral angle of Ant unit of **4c**. (e) Side and diagonal views of TMS-group containing non-planar Ant unit, expansion of red-dashed square in (d). Hydrogens are omitted for clarity.

### UV-vis absorption and emission spectroscopy, and cyclic voltammetry

UV-vis absorption and emission spectroscopy was utilized to explore relationships that exist between the unique structural features and optical properties of **4a-c**. The UV-vis spectrum of **4a** in  $CH_2Cl_2$  (Figure 3 and Table 1) contains a distinctive pattern of peaks at almost identical wavelengths as those in the spectrum of 1,2-di(9-anthryl)benzene **1a**. This observation indicates that the  $\pi$ -conjugation lengths in **1a** and **4a** are the same because of separation of the Ant  $\pi$ -systems caused by the large dihedral angle to the central benzene ring. On the other hand, **4b-c** display 10 nm red-shifted absorptions compared to that of **4a** owing to an increase in intramolecular interactions between the Ant rings brought about by substitution at 10-position of anthracene unit.<sup>[6b]</sup> In addition, the molar extinction coefficients of **4b-c** are >2-fold larger than that of **1a** likely a result of the same effect. The

fluorescence spectrum of **4a** contains an excimer emission band centered at 510 nm and an emission quantum yield ( $\Phi_{em}$ ) of 7%, which are both almost identical to those of **1a**. The emission maximum of **4b** is in the range of that of **4a**, but emission from **4c** is slightly blue-shifted (490-505 nm). The differences are a consequence of interference with excimer formation brought about by the bulky TMS substituents on the Ant unit. Owing to the fact that they do not undergo intramolecular photocycloaddition (see below), **4b** and **4c** have larger  $\Phi_{em}$  values of 31 and 46%, respectively.

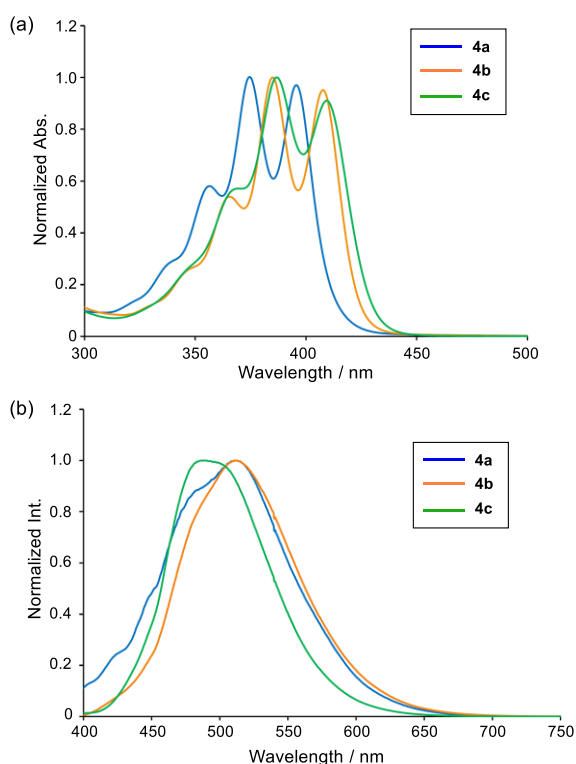


**Figure 3.** (a) Normalized UV-vis spectra of **4a** (blue), **4b** (orange) and **4c** (green) in  $\text{CH}_2\text{Cl}_2$ . (b) Normalized Emission spectra of **4a** (blue), **4b** (orange) and **4c** (green) in  $\text{CH}_2\text{Cl}_2$ .

**Table 1.** Absorption ( $\lambda_{abs}$ ) peaks, molar coefficients ( $\epsilon$ ), emission ( $\lambda_{em}$ ) peaks, and emission quantum yields ( $\Phi_{em}$ ) of **4a-c** and **1a** in  $\text{CH}_2\text{Cl}_2$  solution.

	$\lambda_{abs}$ / nm	$\epsilon$ / $\text{M}^{-1} \text{cm}^{-1}$	$\lambda_{em}$ / nm	$\Phi_{em}$ / %
<b>4a</b>	396, 375, 356	---[b]	510, 480 (sh)	7
<b>4b</b>	408, 385, 366	46500	510	31
<b>4c</b>	409, 387, 369	42100	505 (sh), 490	46
<b>1a</b> [a]	395, 370, 355	18200	510, 480 (sh)	6

[a] ref. [6a]. [b] Difficult to determine due to its insolubility.

To gain information about redox properties, cyclic voltammetry studies were carried out with **4b** and **4c**. Inspection of the voltammograms (Figure 4)<sup>[12]</sup> showed that the first oxidation

potential ( $E^{1/2}$  vs.  $\text{Fc}/\text{Fc}^+$ ) of **4b** is +0.60 V whereas that of **4c** is +0.67 V, a difference that is caused by the electron deficient nature of silicon in the TMS group. Although the first oxidation potential of **4b** is comparable to that of alkyl substituted 1,2-di(9-anthryl)benzene **1b**, the difference between the ( $\Delta E_p$ ) of anodic oxidation peak  $E_{pa}$  and cathodic reduction peak  $E_{pc}$  potentials in **4b** is 180 mV, which is larger than that in **1b** (110 mV, Figure S8). A large  $\Delta E_p$  is also observed for **4c** ( $\Delta E_p = 176$  mV). These phenomena are likely associated with the occurrence of one-step two-electron oxidation of **4b** and **4c** that generates radical cation Ant-dimers on both-sides of the benzene ring. Because no splitting but only broadening of the oxidation wave occurs, electronic interactions between the two radical cation Ant-dimers through the central benzene ring must be small. Also, second oxidation peaks  $E^2$  are observed in the voltammograms of **4b** and **4c** at +1.00 V and +1.10 V, but the waves are irreversible (Figure S9). Notably, the voltammogram of **1b** contains a semi-reversible second oxidation wave (Figure S8), indicating that higher oxidation states of **4b** and **4c** are more reactive than that of **1b**.

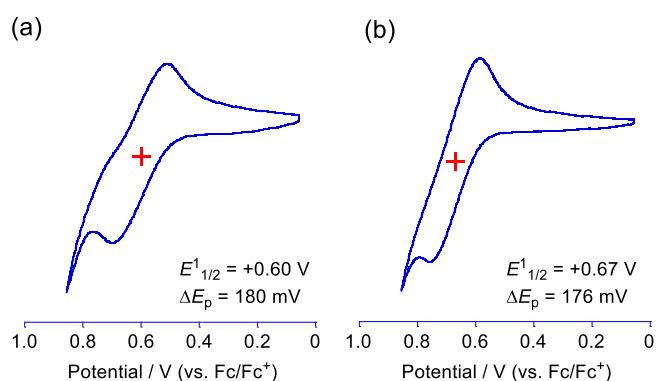


**Figure 4.** Cyclic voltammograms. (a) First oxidation wave  $E^{1/2}$  of **4b**. (b) First oxidation wave  $E^{1/2}$  of **4c** both in  $\text{CH}_2\text{Cl}_2$  with 0.1 M  $^n\text{Bu}_4\text{NPF}_6$  and scan rate = 100  $\text{mV s}^{-1}$ .

### Intramolecular photocycloaddition reactions of **4a**

In previous investigations,<sup>[6]</sup> we observed that **1a** and **2a** undergo photo-induced intramolecular [4+4] cycloaddition between two anthracene units to produce highly strained products containing unusually long C-C single bonds. These results stimulated a study of the photochemical behavior of **4a-c**. The results revealed that photoirradiation ( $\lambda = 365$  nm) of **4b-c** in solutions does not promote observable photoreactions. In contrast, irradiation of a precipitate of **4a** in dichloromethane slowly generates the photoisomer **4a-PI**. During this process, single crystals of **4a-PI** grow in the solution, enabled us to elucidate the unique structure of **4a-PI** using X-ray analysis. Inspection of plots of the X-ray crystallographic data (Figure 5)

shows that **4a-PI** is a bis-[4+4] cycloaddition product in which the central benzene has a distorted planar structure with close to  $D_{2h}$  symmetry.<sup>[13]</sup> The bond lengths in the central benzene ring are only slightly different ( $a = 1.389$  Å,  $b = 1.401$  Å, and  $c = 1.393$  Å), but the internal angles differ significantly from the usual  $120^\circ$  to  $123.8^\circ$  ( $\theta_1$  and  $\theta_2$ ) and  $112.5^\circ$  ( $\theta_3$ ) as a consequence of the presence of fused four-membered rings. In addition, **4a-PI** has an extremely long ( $1.716(3)$  Å) C9-C9' bond<sup>[14]</sup> which exceeds those present in the intramolecular photocycloaddition products of **1a** ( $1.688$  Å) and **2a** ( $1.678$  Å).

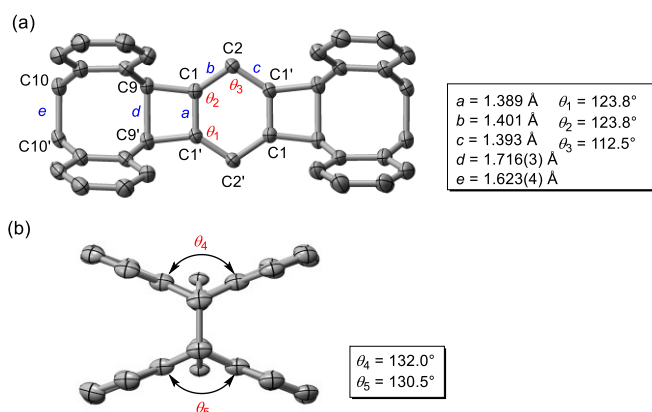


**Figure 5.** Plots of X-ray crystallographic data of **4a-PI**. (a) Side view with selected bond lengths ( $a$ - $e$ ) and internal angle of the central benzene ring ( $\theta_1$ - $\theta_3$ ). (b) Front view with bent angles of anthracene dimer unit ( $\theta_4$ ,  $\theta_5$ ). Hydrogens are omitted for clarity.

It is noteworthy that computationally optimized structures of **4a-PI** obtained using  $\omega$ B97X-D, M06-2X and B3LYP-D3 functionals do not well reproduce the extremely long  $>1.70$  Å C9-C9' bond, but rather give lengths of 1.660 to 1.694 Å for the C9-C9' bond (Figure S10). In addition, these calculated long C-C bond lengths are not extended from those of **1a-PI** (Figure S11), indicating that **4a-PI** does not have the sciccor effect<sup>[14c]</sup> of introducing strained 4-membered rings on both sides of the benzene ring to extend the length of the C9-C9' bond. Therefore, calculated potential energy curves (PECs) of **4a-PI** with C9-C9' bond lengths ranging from 1.60 to 1.75 Å were generated by using the above functionals. The results show that the PECs are relatively shallow and the energy difference between calculated structures with a C9-C9' bond length of 1.72 Å and a length corresponding to the most stable structure being less than 0.75 kcal mol<sup>-1</sup> (Figure 6). The findings indicate that the small strain energy in **4a-PI** can be compensated by intermolecular interactions in crystalline state, and that the length of the C9-C9' bond is highly variable.

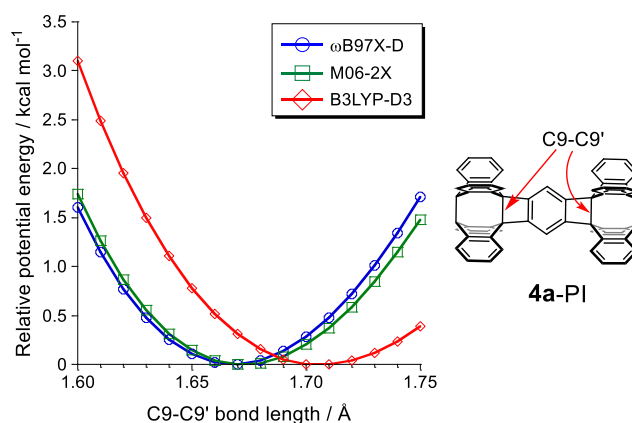


**Figure 6.** Relative PECs of **4a-PI** for C9-C9' bond length computed using  $\omega$ B97X-D, M06-2X, and B3LYP-D3 functional (basic set is 6-31G\*).

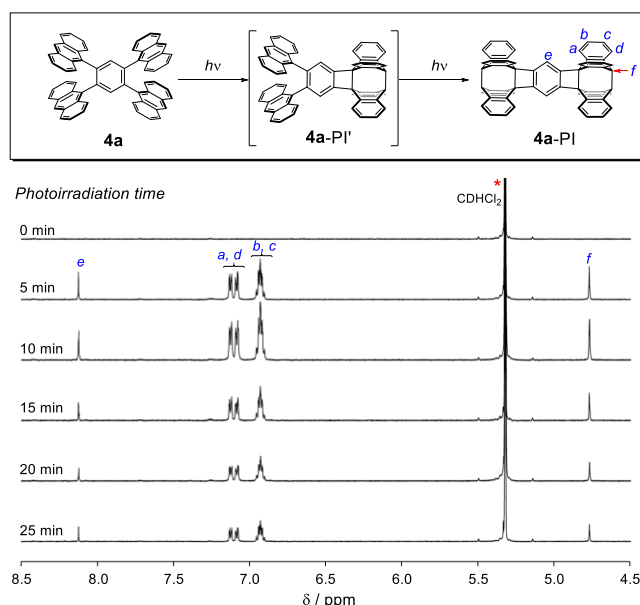


**Figure 7.** Photoirradiation-time dependent <sup>1</sup>H NMR spectra during the conversion of **4a** to **4a-PI** in CD<sub>2</sub>Cl<sub>2</sub> ( $\lambda = 365$  nm).

Owing to the presence of two sites for intramolecular [4+4] cycloaddition in **4a**, we explored the process in more detail to determine whether the mono-cycloaddition intermediate **4a-PI'** is produced initially and if it can be isolated. Quantum chemical calculations reveal that the excited state of **4a** has a stable  $C_1$  structure, in which an anthracene dimer excimer exists on one side and not on the other (Figure S12). The result suggests that photoreaction of **4a** should proceed in a stepwise manner involving initial formation of **4a-PI'** followed by its conversion to **4a-PI**. To assess the validity of this proposal, photoirradiation-time dependent <sup>1</sup>H NMR measurements of **4a** were carried out (Figure 7). Owing to the low solubility of **4a**, no peaks are observed in the <sup>1</sup>H NMR spectrum obtained at 0 min but sharp signals attributed to **4a-PI** arise after photoirradiation begins. However, even after only 5 min photoirradiation, no signals that

can be attributed to **4a-PI** arise in the  $^1\text{H}$  NMR spectrum, probably because this mono-cycloaddition product also has low solubility.

As part of this phase of our studies, we explored the C-C bond dissociation properties of **4a-PI**. The results of differential scanning calorimetry (DSC) showed that in the solid state **4a-PI** undergoes gradual C-C bond dissociation at ca. 150 °C, in conjunction with two exothermic peaks at 165 and 179 °C when the heating rate is 10 °C min $^{-1}$  (Figure 8). In contrast, the DSC plot of **1a-PI** contains one broad exothermic peak at 172 °C (Figure S14). Thus, the two exothermic peaks in the DSC of **4a-PI** likely correspond to C-C bond dissociation taking place at the two sites where intramolecular photocycloaddition has taken place. It would have been interesting to know whether the first bond dissociation event on one side has an impact on the second C-C bond dissociation event on the another side. However, the bond dissociation events at the two sites seem to occur independently because the peak intensity of first exothermic peak at 165 °C is greater than that of second exothermic peak at 179 °C. If the bond dissociation event occurs in a tandem stepwise fashion, the ratio of the intensities of the two exothermic peaks should be 1:1. The experimental value of the energy difference ( $\Delta H_{\text{iso}}$ ) between **4a** and **4a-PI** is 28.2 kcal mol $^{-1}$ , which is only 1.2 times larger than that between **1a** and **1a-PI** (23.3 kcal mol $^{-1}$ ). Although computational determinations of the energy differences between **4a** and **4a-PI** as well as **1a** and **1a-PI** were performed, the experimental results were not reproduced (Figure S13). The reason(s) for the differences is not clear, but it appears that intermolecular interactions in **4a-PI** or **1a-PI** in solid state affect the  $\Delta H_{\text{iso}}$  values.

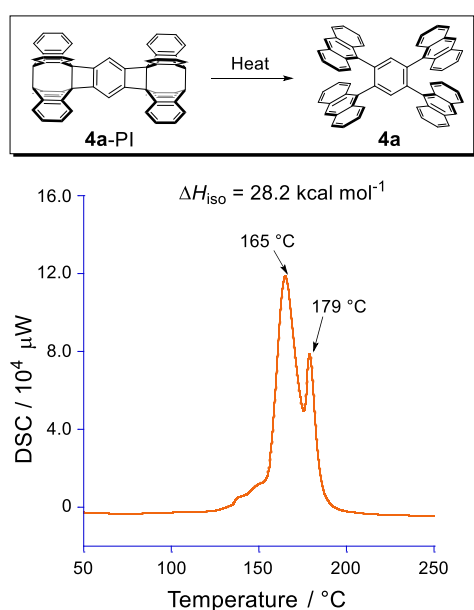


**Figure 8.** The DSC plot of **4a-PI** (heating rate: 10 °C/min) and the energy difference ( $\Delta H_{\text{iso}}$ ) between **4a** and **4a-PI**.

## Charge-transfer complexes and exciplex emission

In the final phase of this investigation, we assessed the occurrence and effects of donor-acceptor interactions between **4a-c** and several acceptors. The  $\pi$ -congested arrangement of aromatic rings can lead to an enhanced electron donor ability, and possibly facilitate charge-transfer (CT) complex formation. Recently, it was reported that several CT complexes exhibit an exciplex emission<sup>[15]</sup> in the form of thermally-activated delayed fluorescence (TADF)<sup>[16, 17]</sup> because molecular orbital distributions of HOMOs and LUMOs in these complex are located on respective donor and acceptor molecules. This approach for generating TADF is highly attractive because CT complexes can be prepared by simple mixing of donor and acceptor molecules. In addition, we also envisioned that CT complexes between **4a** and acceptors would have unique 2D packing structures in the crystal state.

In an exploration to test these proposals, we observed that CT complexation does not take place between **4a** and several acceptors such as 7,7,8,8-tetracyanoquinodimethane (TCNQ), 2,3,5,6-tetrafluoro-7,7,8,8-tetracyanoquinodimethane ( $F_4$ -TCNQ), or 1,2,4,5-tetracyanobenzene (TCNB) owing to the **4a** insolubility issue. Although the CT complexation between **4c** and the above acceptors also does not occur, **4b** does form CT complexes with  $F_4$ -TCNQ and TCNB, whose single crystals are suitable for the X-ray analysis. Plots of the crystallographic data (Figure 9) show the acceptors in the complexes are not located in the space between the two adjacent Ant units in **4b** but rather they are positioned on the outside of Ant units. The complexation ratios between **4b** and  $F_4$ -TCNQ and TCNB are 1:2 and 2:3, respectively. In addition, the acceptor molecules are sandwiched between two **4b** molecules in the form of a donor-acceptor-donor arrangement (Figure S5). In both complexes, the acceptors  $F_4$ -TCNQ and TCNB exist in three independent (A, B, and C) and two independent molecules (A and B), respectively. The distances between the acceptor and Ant planes are 3.34-3.39 Å for  $F_4$ -TCNQ and 3.36-3.40 Å for TCNB, which are usual  $\pi$ - $\pi$  stacking distances. Moreover, the  $C_{9a}\cdots C_{9a}'$ ,  $C_{9b}\cdots C_{9b}'$ ,  $C_{10a}\cdots C_{10a}'$  and  $C_{10b}\cdots C_{10b}'$  distances between adjacent Ant-Ant moieties are not observably different in the complexes, and they are also similar to those un-complexed **4b** (Figure 2b).

Solid state diffuse reflectance UV-vis spectroscopy was employed to evaluate the optical properties of the CT complexes (Figure 10). The spectrum of the CT complex between **4b** and  $F_4$ -TCNQ contains a broad CT absorption band in the near-infrared (NIR) region (1330 and 1100 nm) whereas the spectrum of the complex between **4b** and TCNB contains a narrower CT



absorption band in the visible region (580 nm). Based on the redox potential of **4b** and those of the acceptors, the CT absorption wavelengths are well fitted using a Torrance V-shaped correlation (Figure S15),<sup>[18]</sup> indicating that the enhanced donor ability of the two adjacent Ant units affects the wavelength maximum of the CT band. Because the complex between **4b** and F<sub>4</sub>-TCNQ, displays NIR absorption, the degree of ionicity was evaluated using the bond length alternation of F<sub>4</sub>-TCNQ observed in the crystal of the CT complex (Figure S16).<sup>[19]</sup> The results show that almost no ionic character exists in the B and C molecules of F<sub>4</sub>-TCNQ, and small ionic character of about -0.31 is present in the A molecule of F<sub>4</sub>-TCNQ (Figure 9a). IR analysis of the CT crystals shows that the band associated with C≡N stretching in F<sub>4</sub>-TCNQ undergoes a small shift upon complex formation (Figure S17), again indicating the creation of only a small degree of ionic character.

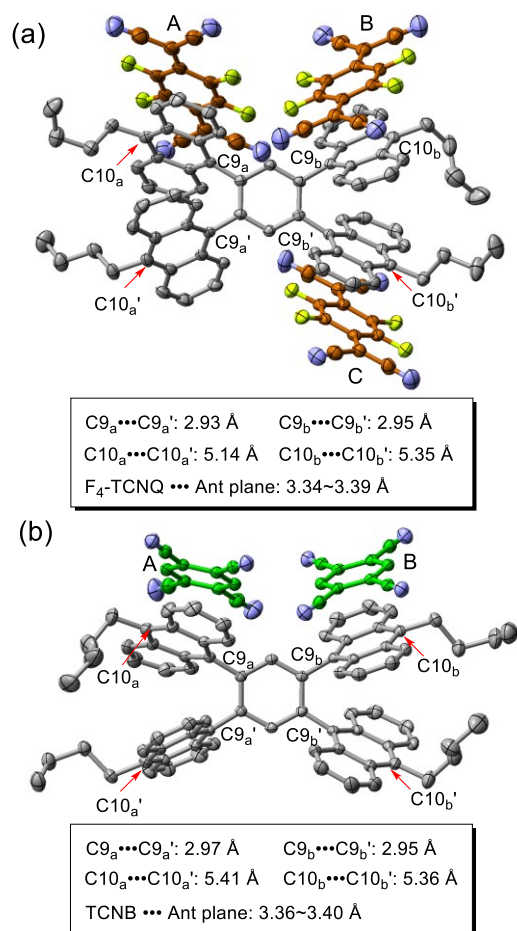


**Figure 9.** Plots of X-ray crystallographic data of CT complexes of **4b**. (a) Complex of **4b** and F<sub>4</sub>-TCNQ. Three independent F<sub>4</sub>-TCNQ molecules (A, B, and C) are present in the crystal. The color of the carbon-frame of F<sub>4</sub>-TCNQ is represented as orange. (b) Complex of **4b** and TCNB. Two independent TCNB molecules (A and B) are present in the crystal. The color of the carbon-frame of TCNB is represented as green. Hydrogens are omitted for clarity.

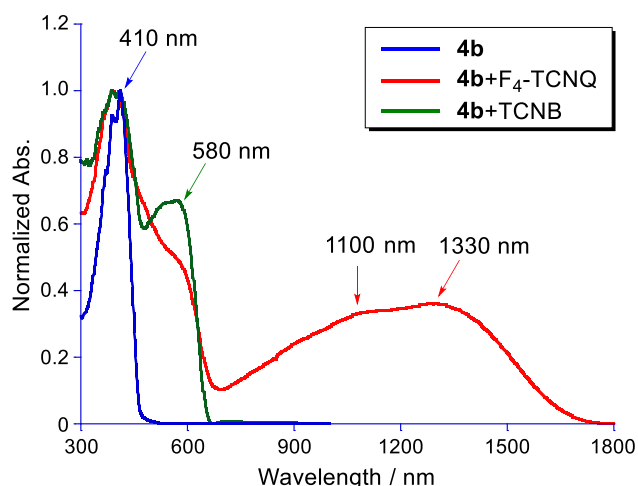


**Figure 10.** Solid state diffuse reflectance UV-vis-NIR spectra of **4b**, **4b**+F<sub>4</sub>-TCNQ, and **4b**+TCNB.

Although exciplex emission from the complex between **4b** and F<sub>4</sub>-TCNQ is difficult to measure because the CT absorption band is >1000 nm, dark red colored emission from the complex between **4b** and TCNB can be observed (Figure 11a). However, the single crystal of the CT complex between **4b** and TCNB was obtained as mixture also containing crystals of un-complexed **4b** and TCNB, with the CT crystal being a minor component. Thus, accumulating important information such as the emission quantum yield and lifetime of the exciplex from **4b** and TCNB is not possible.

We found a unique emission shift takes place upon cooling the CT crystal (Figure 11b). For example, at 0 °C, the exciplex emission wavelength maximum is 680 nm, which is close to NIR region, and the maximum gradually blue-shifts and the intensity increases upon cooling reaching 675 nm at -40 °C, 668 nm at -80 °C and 665 nm at -120 °C. These findings indicate that structural relaxation of the excited state of the complex between **4b** and TCNB is suppressed by cooling, resulting in the hypsochromic shift.<sup>[20]</sup> Therefore, its exciplex emission makes this complex applicable as a thermochromic material.<sup>[21, 22]</sup>

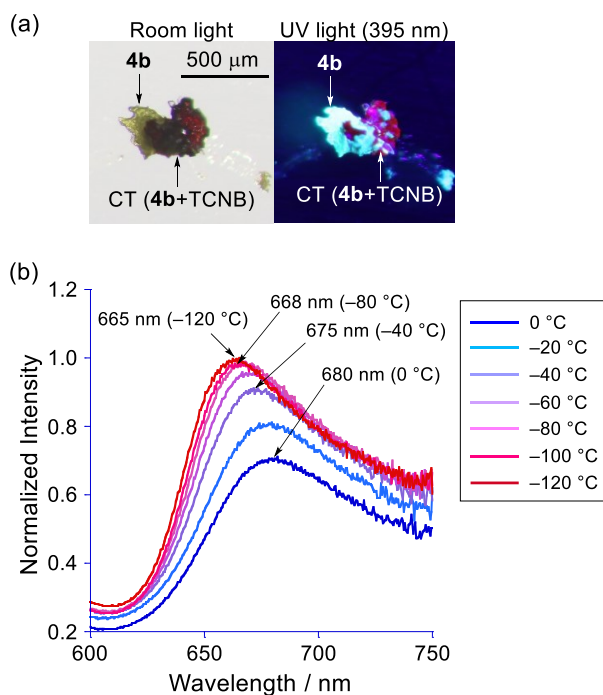


**Figure 11.** (a) Photographic images of the crystal of CT complex between **4b** and TCNB under room light (left) and under UV light (395 nm, right). (b) Temperature dependency of the exciplex emission of **4b** and TCNB from 0 °C to -120 °C ( $\lambda_{\text{ex}} = 450 \text{ nm}$ ).

## Conclusion

X-shaped  $\pi$ -congested substances **4a-c**, containing four Ant units were synthesized in this study. Analysis of the crystal packing structure of **4a** showed it is comprised of a highly-ordered 2D network of X-shaped molecules, in which many intermolecular CH- $\pi$  and  $\pi$ - $\pi$  interactions occur. Photoirradiation to **4a** produces the strained intramolecular photocycloaddition product **4a-PI** that possesses a very long 1.700 Å C-C bond. Co-crystallization of **4b** with the acceptors  $F_4$ -TCNQ or TCNB gives rise to crystalline CT complexes, in which alternative donor-acceptor arrangements occur. In addition, the CT complexes display NIR absorption and exciplex emission. The observations made in this effort are important because they lead to a greater understanding of the properties of other anthracene-accumulated  $\pi$ -clusters such as 1,2,3,4-tetra(9-anthryl)benzene **3** and **HAntB**, whose synthesis is being explored in ongoing studies.

## Experimental Section

Experimental procedures for the synthesis of all compounds, characterization data, and X-ray crystallographic details are pro-

vided in the Supporting Information. Deposition Numbers: 2157951 (for **4a**), 2157952 (for **4b**), 2157953 (for **4c**), 2192879 (for **4a-PI**), 2195284 (for **4b** and  $F_4$ -TCNQ), and 2195283 (for **4b** and TCNB) contain the supplementary crystallographic data for this paper. These data are provided free of charge by the joint Cambridge Crystallographic Data Centre and Fachinformationszentrum Karlsruhe <http://www.ccdc.cam.ac.uk/structures> Access Structures service.

## Acknowledgements

T. N. would like to thank Prof. Takumi Konno and Prof. Nobuto Yoshinari (Osaka Univ.) for help in measuring emission and excitation spectra, and Prof. Shuichi Suzuki (Osaka Univ.) for help in measuring HR-MS,  $^1\text{H}$ - and  $^{13}\text{C}$ -NMR, DSC. Single crystal X-ray crystallographic measurements were performed at the Analytical Instrument Facility, Graduate School of Science, Osaka University. Computations were performed using Research Center for Computational Science, Okazaki, Japan (Project: 22-IMS-C208). This work was supported by JSPS KAKENHI Grant-in-Aid for Scientific Research (C) JP20K05475 (T. N.), Transformative Research Areas (A) JP20H05865 (T.K.), and JP21H05482 (S.S.).

## Conflict of Interest

The authors declare no conflict of interest.

**Keywords:**  $\pi$ -cluster • anthracene • CH- $\pi$  interaction • photoisomerization • charge-transfer complex

- [1] a) C. J. Brown, A. C. Farthing, *Nature* **1949**, *164*, 915; b) D. J. Cram, H. Steinberg, *J. Am. Chem. Soc.* **1951**, *73*, 5691; c) J. H. Golden, *J. Chem. Soc.* **1961**, 3741; d) D. J. Cram, J. M. Cram, *Acc. Chem. Res.* **1971**, *4*, 204; e) T. Umemoto, S. Satani, Y. Sakata, S. Misumi, *Tetrahedron Lett.* **1975**, *16*, 3159; f) R. H. Mitchell, R. J. Carruthers, J. C. M. Zwinkels, *Tetrahedron Lett.* **1976**, *17*, 2585; g) H. Inrgarter, R. G. H. Kirrstetter, C. Krieger, H. Rodewald, H. A. Staab, *Tetrahedron Lett.* **1977**, *18*, 1425; h) S. Misumi, T. Otsubo, *Acc. Chem. Res.* **1978**, *11*, 251; i) T. Tsuji, M. Ohkita, T. Konno, S. Nishida, *J. Am. Chem. Soc.* **1997**, *119*, 8425.
- [2] F. Diederich in *Cyclophanes*, The Royal Society of Chemistry: London, **1991**.
- [3] For typical examples of excimer emission at room temperature, see; a) H. B. -Laurent, A. Castellan, J. -P. Desvergne, R. Lapouyade, *Chem. Soc. Rev.* **2001**, *30*, 248; b) Y. Wu, M. Frascioni, D. M. Gardner, P. R. McGonigal, S. T. Schneebeli, M. R. Wasielewski, J. F. Stoddart, *Angew. Chem. Int. Ed.* **2014**, *53*, 9476.



- [4] For typical examples of photoisomerization in  $\pi$ -congested system, see; a) T. Toyoda, A. Iwama, Y. Sakata, S. Misumi, *Tetrahedron Lett.* **1975**, 16, 3203; b) H. Higuchi, E. Kobayashi, Y. Sakata, S. Misumi, *Tetrahedron*. **1986**, 42, 1731.
- [5] a) F. Schlütter, T. Nishiuchi, V. Enkelmann, K. Müllen, *Polym. Chem.* **2013**, 4, 2963; b) T. Nishiuchi, S. Aibara, T. Kubo, *Angew. Chem. Int. Ed.* **2018**, 57, 16516; c) T. Nishiuchi, K. Kisaka, T. Kubo, *Angew. Chem. Int. Ed.* **2021**, 60, 5400; d) T. Nishiuchi, D. Ishii, S. Aibara, H. Sato, T. Kubo, *Chem. Commun.* **2022**, 58, 3306; e) T. Nishiuchi, S. Aibara, T. Yamakado, R. Kimura, S. Saito, H. Sato, T. Kubo, *Chem. Eur. J.* **2022**, 28, e202200286.; f) T. Nishiuchi, S. Aibara, H. Sato, T. Kubo, *J. Am. Chem. Soc.* **2022**, 144, 7479.
- [6] a) T. Nishiuchi, S. Uno, Y. Hirao, Y. Kubo, *J. Org. Chem.* **2016**, 81, 2106; b) T. Nishiuchi, H. Sotome, K. Shimizu, H. Miyasaka, T. Kubo, *Chem. Eur. J.* **2022**, 28, e202104245.
- [7] a) I. Dance, M. Scudder, *J. Chem. Soc. Chem. Commun.* **1995**, 1039.; b) I. Dance, M. Scudder, *Chem. Eur. J.* **1996**, 2, 481.; c) I. Dance, M. Scudder, *CrystEngComm.* **2009**, 11, 2233.
- [8] T. Nishiuchi, H. Sotome, R. Fukuuchi, K. Kamada, H. Miyasaka, T. Kubo, *Aggregate* **2021**, 2, e126.
- [9] Although tetra(9-anthryl) substituted benzenes have not been reported, several molecules having four Ant units with close inter-planar distance have been reported, see; a) S. Toyota, M. Goichi, M. Kotani, *Angew. Chem. Int. Ed.* **2004**, 43, 2248; b) S. Aoki, E. Tsurumaki, M. Yamashita, K. Wakamatsu, S. Toyota, *ChemPlusChem*, **2022**, 87, e202100447.
- [10] a) M. Aufiero, T. Sperger, A. S. -K. Tsang, F. Schoenebeck, *Angew. Chem. Int. Ed.* **2015**, 54, 10322; b) I. Kalvet, G. Magnin, F. Schoenebeck, *Angew. Chem. Int. Ed.* **2017**, 56, 1581.
- [11] The distorted Ant unit is also observed in 9-*tert*-butylantracene, see; K. Angermund, K. H. Claus, R. Goddard, C. Krüger, *Angew. Chem. Int. Ed.* **1985**, 24, 237.
- [12] Due to the insolubility of **4a**, the measurement of CV could not be conducted.
- [13] A similar  $D_{2h}$  distorted benzene ring exists in [3]phenylene, see; B. C. Berris, G. H. Hovakeemian, Y. -H. Lai, H. Mestdagh, K. P. C. Vollhardt, *J. Am. Chem. Soc.* **1985**, 107, 5670.
- [14] For selected compounds possessing long C-C single bonds over 1.700 Å, see; a) K. Tanaka, N. Takamoto, Y. Tezuka, M. Kato, F. Toda, *Tetrahedron*, **2001**, 57, 3761.; b) P. R. Schreiner, L. V. Chernish, P. A. Gunchenko, E. Y. Tikhonchuk, H. Hausmann, M. Serafin, S. Schlecht, J. E. P. Dahl, R. M. K. Carlson, A. A. Fokin, *Nature*, **2011**, 477, 308.; c) Y. Ishigaki, T. Shimajiri, T. Takeda, R. Katoono, T. Suzuki, *Chem*, **2018**, 4, 795.; d) J. Li, R. Pang, Z. Li, G. Lai, X. -Q. Xiao, T. Müller, *Angew. Chem. Int. Ed.* **2019**, 58, 1397.; e) T. Kubo, Y. Suga, D. Hashizume, H. Suzuki, T. Miyamoto, H. Okamoto, R. Kishi, M. Nakano, *J. Am. Chem. Soc.* **2021**, 143, 14360.
- [15] For selected papers of exciplex emission, see; a) M. R. Wasielewski, *Chem. Rev.* **1992**, 92, 435.; b) N. Mataga, H. Chosrowjan, S. Taniguchi, *J. Photochem. Photobiol., C*, **2005**, 6, 37-79.; c) J. Guo, Y. Zhen, H. Dong, W. Hu, *J. Mater. Chem. C* **2021**, 9, 16843.; d) X. Yan, H. Peng, Y. Xiang, J. Wang, L. Yu, Y. Tao, H. Li, W. Huang, R. Chen, *Small*, **2022**, 18, 2104073.
- [16] For selected papers of TADF, see; a) C. A. Parker, C. G. Hatchard, *Trans. Faraday Soc.* **1961**, 57, 1894.; b) A. Maciejewski, M. Szymanski, R. P. Steer, *J. Phys. Chem.* **1986**, 90, 6314.; c) A. Endo, K. Sato, K. Yoshimura, T. Kai, A. Kawada, H. Miyazaki, C. Adachi, *Appl. Phys. Lett.* **2011**, 98, 083302.; d) H. Uoyama, K. Goushi, K. Shizu, H. Nomura, C. Adachi, *Nature*. **2012**, 492, 234.; e) T. Hatakeyama, K. Shiren, K. Nakajima, S. Nomura, S. Nakatsuka, K. Kinoshita, J. Ni, Y. Ono, T. Ikuta, *Adv. Mater.* **2016**, 28, 2777.; f) Z. Yang, Z. Mao, Z. Xie, Y. Zhang, S. Liu, J. Zhao, J. Xu, Z. Chi, M. P. Aldred, *Chem. Soc. Rev.* **2017**, 46, 915.
- [17] For a CT complex with a TADF property, see; a) H. -Y. Zhou, D. -W. Zhang, M. Li, C. -F. Chen, *Angew. Chem. Int. Ed.* **2022**, 61, e202117872.; b) S. Garain, S. N. Ansari, A. A. Kongasseri, B. C. Garain, S. K. Pati, S. J. George, *Chem. Sci.* **2022** (DOI: 10.1039/d2sc03343g)
- [18] J. B. Torrance, J. E. Vazquez, J. J. Mayerle, V. Y. Lee, *Phys. Rev. Lett.* **1981**, 46, 253.
- [19] a) T. J. Kistenmacher, T. J. Emge, A. N. Bloch, D. O. Cowan, *Acta. Cryst.* **1982**, B38, 1193.; b) A. L. Sutton, B. F. Abrahams, D. M. D'Alessandro, R. W. Elliott, T. A. Hudson, R. Robson, P. M. Usov, *CrystEngComm*, **2014**, 16, 5234.
- [20] R. A. Krueger, G. Blanquart, *J. Phys. Chem. A* **2019**, 123, 1796.
- [21] Thermochromic exciplex emission, see; D. Inamori, H. Masai, T. Tamaki, J. Terao, *Chem. Eur. J.* **2020**, 26, 3385.
- [22] For selected papers of thermochromic materials, see; a) C. Reichardt, *Chem.Soc. Rev.* **1992**, 21, 147.; b) A. Seeboth, D. Lötzsche, R. Ruhmann, O. Muehling, *Chem. Rev.* **2014**, 114, 3037.